Tetra-orientated Mamba with T2-FLAIR Mismatch Features for Glioma Segmentation, IDH Genotyping, and Grading

Xinyu Li[1], Jin Liu*[1], Hulin Kuang[1] , Yuanzhuo Wang[1], and Jianxin Wang[1]

[1] Hunan Provincial Key Lab on Bioinformatics, School of Computer Science and Engineering, Central South University, Changsha 410083, Hunan, China
liujin06@csu.edu.cn

Abstract. Tumor grading and Isocitrate Dehydrogenase (IDH) status are key prognostic biomarkers. Transformer-based methods are widely applied in glioma segmentation and diagnosis, but challenges still exist due to the tumor's heterogeneity and the computational burden of Transformers. We propose a multi-task network called MTamba for glioma segmentation, IDH genotyping, and grading. We design Tetra-oriented Mamba to perform global information interaction from different orientations in MRIs for segmentation. We design a T2-FLAIR mismatch feature extraction module to explore the mismatch features between T2 and FLAIR images at different depths to enhance diagnosis. We propose a channel-space Siamese Mamba fusion module to fuse T2-FLAIR mismatch features with multimodal MRI features from the segmentation encoder for diagnosis. Finally, we apply an uncertainty loss optimization method to jointly optimize glioma segmentation, IDH genotyping, and grading. We validate MTamba on the publicly available UCSF-PDGM and BraTS2020 datasets, and experimental results show that MTamba outperforms existing multi-task learning methods. The code for MTamba is available at https://github.com/xhwv/MTamba.

Keywords: Glioma · Mamba · Multi-task learning · Segmentation · IDH genotyping · Grading.

1 Introduction

Gliomas are common and deadly brain tumors. According to the WHO classification, survival rates and treatment responses are closely linked to isocitrate dehydrogenase (IDH) mutation status and tumor grade [20]. Traditionally, genetic information is obtained through biopsy or surgery, which can delay treatment and increase metastasis risk. In contrast, multimodal MRI offers non-invasive, complementary information, making it a promising alternative [8].

Transformers are commonly used in visual tasks, but their computational complexity limits their use in medical image analysis. State-space models (SSMs),

* means the corresponding author.

especially the Structured State Space (S4) model, offer an efficient alternative [9]. The Tri-orientated Mamba (ToM) in Segmamba performs well in interacting with 3D features across spatial orientations [22], but struggles with channel and long-range dependencies between distant slices. Improving Mamba's ability to capture long-range dependencies could enhance global modeling of medical images.

The features extracted from the glioma segmentation encoder contain information about the tumor's edges and location, which is useful for prognosis [4, 18, 7, 23]. The incidence of IDH mutations is approximately 12% in WHO grade 4 gliomas and nearly 60% in grade 3 gliomas, indicating a complementary relationship between IDH genotyping and grading [2]. Thus, performing segmentation, IDH typing, and grading simultaneously may be an efficient strategy.

T2-FLAIR mismatch signals are vital for glioma IDH genotyping and grading [11]. Gliomas typically show hyperintensity on T2 and hypointensity on FLAIR images. IDH-mutant and lower-grade gliomas are often linked to mismatch signals [14]. Previous methods rely on T2-FLAIR subtraction, and it is hard to capture subtle inter-modality differences [24, 6]. Introducing attention can help models focus on key regions and capture relationships between modalities. T2-FLAIR mismatch signals are not always present in IDH-mutant gliomas, and combining them with multimodal MRI features is essential for diagnosis.

This paper proposes MTamba, a multi-task network integrated with Mamba, designed to perform glioma segmentation, IDH genotyping, and grading simultaneously. Our main contributions are summarized as follows:

1) We propose the Tetra-orientated Mamba (TeoM) as the core module of MTamba to enhance the exploration of global information by interacting with sequences flattened from 3D features in four orientations.

2) We design the T2-FLAIR Mismatch Feature Extraction Module, which adjusts the focus areas on T2 and FLAIR images using multi-scale share-weighted convolutions, capturing shallow T2-FLAIR mismatch features. We use a TeoM-based feature extractor to explore deep T2-FLAIR mismatch features.

3) We design a channel-spatial siamese mamba fusion module, performing global interaction of T2-FLAIR mismatch and multimodal MRI features across channel and spatial levels, enhancing the expressiveness of fused features.

2 Methodology

As shown in Fig.1, MTamba consists of components: 1) Glioma Segmentation Module: We design the Tetra-oriented Mamba (TeoM) to model global features and segmentation. 2) T2-FLAIR Mismatch Feature Extraction Module: We design shallow and deep mismatch extraction modules for T2-FLAIR mismatch features. 3) Channel-Spatial Siamese Mamba Fusion Module: We fuse T2-FLAIR mismatch features with features from the segmentation module for diagnosis.

2.1 Glioma Segmentation Module

Tumor region information is vital for diagnosis. As shown in Fig.1(a, b), we use SegMamba as the backbone for segmentation. We replace tri-orientated

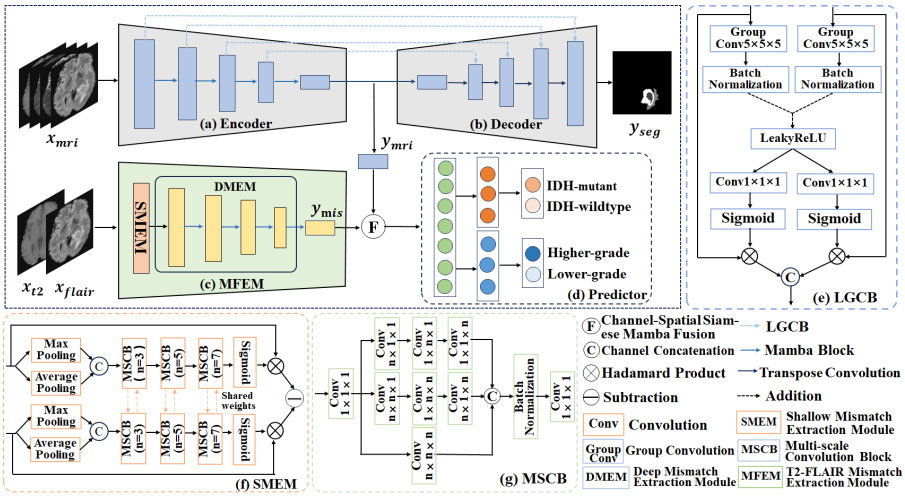

Fig. 1: Overall Pipeline of the Proposed MTamba.

Mamba (ToM) with Tetra-oriented Mamba (TeoM) in the encoder and keep the convolution-based decoder. We obtain segmentation outputs and encoder outputs y_{mri} as multimodal MRI features during segmentation.

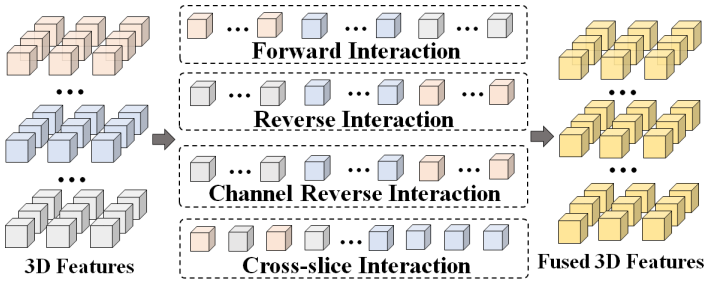

Fig. 2: The Architecture of the Tetra-orientated Mamba.

Tetra-orientated Mamba: The ToM in SegMamba has limitations in capturing long-range dependencies between channels and distant slices. As shown in Fig.2, we propose TeoM, which models global features in four orientations: forward, reverse, channel-reverse, and cross-slice. The forward and reverse interactions are consistent with ToM. Channel-reverse interaction captures dependencies by reversing the channel. Unlike ToM's inter-slice interaction, which gradually scans the slices, TeoM's cross-slice interaction alternately scans the first and last slices, then progressively moves toward the middle slices, enabling

exploration of dependencies between distant slices. TeoM is expressed as:

$$F_{TM}(x) = \sum_{N \in \{f,r,cr,cs\}} W_{mamba}(x_N), \tag{1}$$

where W_{mamba} is Mamba layers. The x_f, x_r, x_{cr}, x_{cs} are input features flattened in forward, reverse, channel-reverse, and cross-slice orientations.

Large-Kernel Gated Convolution Block: SegMamba uses feature-level uncertaint estimation (FUE) with point convolutions to fuse features from encoders (x_{en}) and decoders (x_{de}), making it hard to explore their relationships. We propose a Large Kernel Gated Convolution Block (LGCB), which fuses x_{en} and x_{de} at multi-scales using x_{att} derived from large receptive convolutions:

$$x_{att} = \sigma(\beta(W_g^5(x_{en})) + \beta(W_g^5(x_{de}))), \tag{2}$$

where W_g^5 is a grouped convolution of kernel size 5, σ is the Leaky ReLU, and β is batch normalization. Point convolution and Sigmoid are applied to y_{att} to generate attention coefficients, which are used to weight x_{en} and x_{de}. Finally, the weighted features are concatenated to produce the output of LGCB.

$$y_{lgcb} = (\rho(W_p(x_{att})) \times x_{en}) \oplus (\rho(W_p(x_{att})) \times x_{de}), \tag{3}$$

where W_p is pointwise convolution, ρ denotes the Sigmoid function, $\times$ refers to element-wise multiplication, and $\oplus$ represents channel concatenation.

2.2 T2-FLAIR Mismatch Feature Extraction Module

Shallow Mismatch Extraction: Directly subtracting T2 and FLAIR images will treat all regions equally, missing key mismatch information. Thus, we first use average and max pooling to explore their local context separately.

$$x_i^p = W_p(P_{avg}(x_i) \oplus P_{max}(x_i), \quad i \in \{t2, flair\}) \tag{4}$$

where P_{avg} and P_{max} are average and max pooling, respectively. We use multiple shared-weight multi-scale convolutional blocks (MSCB) to explore complementary information between x_{t2}^p and x_{flair}^p. The process of MSCB is shown as:

$$F_m^n(x_i^p) = W_p(\beta(w_{11n}(w_{1n1}(w_{n11}(x_i^p))) \oplus w_{n1n}(w_{1nn}(w_{nn1}(x_i^p))) \oplus w_{nnn}(x_i^p))), \tag{5}$$

where w_{nnn} are convolutions with a kernel size of $n \times n \times n$. We weight the T2 and FLAIR images with share-weighted MSCBs and then subtract them to obtain the output of the shallow mismatch extraction module (SMEM):

$$y_{smem} = \rho(F_m^7(F_m^5(F_m^3(x_{t2}^p)))) \times x_{t2} - \rho(F_m^7(F_m^5(F_m^3(x_{flair}^p)))) \times x_{flair}, \tag{6}$$

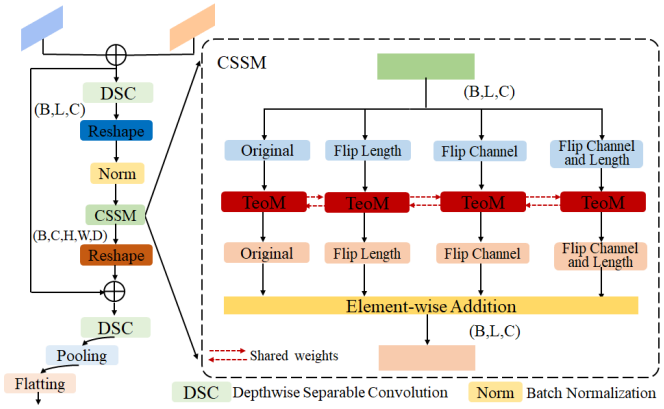

Fig. 3: The Architecture of the Channel-Spatial Siamese Mamba Fusion Module

Deep Mismatch Extraction: We use the same structure as the segmentation encoder for feature extraction on x_{smem} and obtain T2-FLAIR mismatch features y_{mis} as the output of the Deep Mismatch Extraction Module (DMEM).

2.3 Channel-Spatial Siamese Mamba Fusion Module

We propose the Channel-Spatial Siamese Mamba Fusion Module (CSSMF) to fuse y_{mri} and y_{mis} at channel and spatial levels. Specifically, we first add y_{mri} and y_{mis}, then use depthwise separable convolutions (DSC) to capture local information, and reshaped to the shape (B, L, C):

$$y_b = \beta(F_{reshape}^{B,L,C}(W_{dsc}(x_{mri} + y_{mis}))), \tag{7}$$

where W_{dsc} is the depthwise separable convolution, $F_{reshape}^{B,L,C}$ denotes reshaping the feature map from (B, C, H, W, D) into the shape (B, L, C). Next, we input y_b into the Channel-Spatial Siamese Mamba (CSSM) block, where we enhance the y_b across channel and spatial levels. The enhanced features are then processed by the share-weighted TeoM to explore global contextual relationships:

$$y_{cssm} = F_{TM}(y_b) + F_f^l(F_{TM}(F_f^l(y_b))) + F_f^c(F_{TM}(F_f^c(y_b))) + F_f^{lc}(F_{TM}(F_f^{lc}(y_b))), \tag{8}$$

where F_f^l, F_f^c, and F_f^{lc} are flipping in spatial, channel, both spatial and channel dimensions, respectively. Then, we reshape y_{cssm} back to the shape (B, C, H, W, D) and use DSC to enhance features. Finally, we obtain the output of CSMMF by performing pooling along the channel and flattening, which is expressed as:

$$y_{cssmf} = F_{flatten}(P_{avg}^c(W_{dsc}(F_{reshape}^{B,C,H,W,D}(y_{cssm})))), \tag{9}$$

where P_{avg}^c is average pooling along the channel, and $F_{flatten}$ denotes flattening. The fused feature y_{cssmf} is used for IDH genotyping and grading.

3 Experiments and Results

3.1 Dataset

As shown in Tab.1, we use UCSF-PDGM and BraTS2020 datasets [3, 1]. Each sample includes T1, T2, T1CE, and FLAIR images, with their segmentation, IDH status, and grades [18]. 1) For UCSF-PDGM, we split data 8:2 for training (15% for validation) and testing. 2) We use the BraTS2020 training set and validation set for training (15% for validation) and testing, respectively.

Table 1: Summary of the datasets used in this study.

	UCSF-PDGM		BraTS2020	
	Training	Testing	Training	Testing
Subject n	394	99	148	70
Grade				
Lower-Grade (2, 3)	77 [20%]	23 [23%]	64 [43%]	42 [60%]
Higher-Grade (4)	317 [80%]	76 [77%]	84 [57%]	28 [40%]
IDH status				
Wildtype	313 [79%]	77 [78%]	91 [61%]	38 [54%]
Mutant	81 [21%]	22 [22%]	57 [39%]	32 [46%]

3.2 Implementation Details

We conduct experiments on A100 GPUs using Ranger [21] as the optimizer, with a batch size of 2 and an initial learning rate of 0.0002 that decays during training. MRIs are preprocessed by repositioning and zero-mean normalization. Augmentation includes random flipping and cropping to shapes of (128,128,128). We use Dice and weighted cross-entropy losses for segmentation and diagnosis, respectively, and use an uncertain loss weight method [12] for joint optimization. We use Dice, AUC, and accuracy (ACC) to evaluate segmentation and diagnosis.

3.3 Comparison with the State-of-the-Art Methods

We compare MTamba with 1 CNN-based diagnostic method, Tupe-Waghmare et al. (M1)[17], and 7 multi-task methods for segmentation and diagnosis, including 3 hybrid CNN-Transformer methods: MFEFnet (M2) [24], MTTU-Net (M3) [4], and M^{3}CI-Net (M4) [23], as well as 4 CNN-based methods: SGPNet (M5) [19], Sun et al. (M6)[16], Decuyper et al. (M7)[7], and PS-Net (M8) [18]. For a fair comparison, we use the public implementations and specific descriptions from their papers to retrain their networks under the same settings. As shown in Tab. 2, MTamba achieves the best performance. Compared to M1, which performs diagnosis without segmentation, we see increases in IDH genotyping and

grading, likely due to MTamba effectively capturing tumor location information. Compared to M8, MTamba shows increases in segmentation and diagnosis, likely due to our effective exploration of T2-FLAIR mismatch features.

Table 2: Performance comparison with other methods (M)

M	Segmentation DICE			IDH Genotyping		Grading	
	WT	TC	ET	AUC	ACC	AUC	ACC
UCSF-PDGM							
M1	∼	∼	∼	80.40±3	75.76±4	84.25±4	79.80±5
M2	87.16±4	81.07±15	79.74±16	79.19±3	74.75±2	∼	∼
M3	90.04±11	84.33±26	82.01±25	88.50±3	82.83±4	∼	∼
M4	89.53±11	84.62±26	82.07±26	89.68±3	84.85±4	∼	∼
M5	89.16±11	84.07±26	81.74±25	84.26±3	78.79±4	∼	∼
M6	87.72±12	81.75±26	80.14±25	84.73±4	78.79±4	86.84±4	81.82±4
M7	90.41±9	84.16±26	82.51±25	83.37±4	80.81±4	85.26±4	81.82±4
M8	90.33±11	83.82±26	82.06±25	87.20±3	82.83±4	89.53±4	84.85±3
MT	**91.73±9**	**85.94±23**	**84.09±22**	**92.51±2**	**88.89±3**	**92.86±4**	**89.90±3**
BraTS2020							
M1	∼	∼	∼	85.21±5	77.14±6	84.22±5	80.00±6
M2	84.24±6	65.14±18	61.31±22	80.61±3	75.71±4	∼	∼
M3	88.23±10	73.80±26	69.68±30	90.61±3	84.29±4	∼	∼
M4	88.49±9	74.02±26	69.03±32	87.09±4	82.86±4	∼	∼
M5	87.27±10	73.17±25	68.96±32	85.94±4	80.00±5	∼	∼
M6	87.71±11	72.55±26	69.63±32	86.77±4	78.57±5	82.43±4	77.14±5
M7	89.23±11	73.46±24	70.18±32	83.16±4	77.14±5	86.20±3	81.43±4
M8	89.35±11	73.27±25	70.79±31	87.45±3	82.86±4	88.05±4	84.29±4
MT	**90.04±9**	**75.15±22**	**72.43±30**	**92.36±2**	**88.57±4**	**93.42±4**	**90.00±3**

3.4 Ablation Study

We conduct ablation experiments on MTamba using the UCSF-PDGM. We compare the following scenarios: w/o MFEM (S1), where only features from the segmentation encoder are used for diagnosis; w/o SMEM (S2), where T2 and FLAIR images are subtracted and input into DMEM; w/o MSCB (S3), replaced with convolutions of the same kernel size; w/o LGCB (S4), replaced with FUE; w/o CSSMF (S5), replaced with summation fusion; w/o TeoM (S6), replaced with ToM; w/o cross-slice interaction (S7), replaced with inter-slice interaction; w/o Segmentation Decoder (S8), where diagnosis is performed; w/o IDH Genotyping (S9), where segmentation and grading are performed; and w/o Grading (S10), where segmentation and IDH genotyping are performed. As shown in Tab. 3, the results of S1, S2, and S3 show the effectiveness of T2-FLAIR mismatch features for diagnosis, while S4, S5, S6 and S7 show the effectiveness of our proposed modules, and S8, S9, and S10 show the effectiveness of performing segmentation, IDH genotyping and grading simultaneously.

Table 3: The results of ablation study on the UCSF-PDGM dataset.

M	Segmentation DICE			IDH Genotyping		Grading	
	WT	TC	ET	AUC	ACC	AUC	ACC
S1	91.14±11	85.03±24	83.29±23	89.76±3	84.85±4	87.3±4	82.83±4
S2	91.22±10	85.07±27	83.73±25	89.83±2	84.85±4	90.48±6	86.87±3
S3	91.46±10	85.24±25	83.97±24	91.40±2	86.87±3	90.88±6	87.88±3
S4	91.28±10	85.11±24	83.59±23	92.44±2	87.88±4	91.16±6	87.88±3
S5	90.97±10	85.58±23	83.81±22	91.69±2	84.85±4	86.25±6	83.84±4
S6	90.35±11	83.99±26	82.74±25	88.16±2	83.84±4	87.30±6	84.85±4
S7	90.48±10	84.28±26	83.69±23	90.33±3	86.87±5	90.46±5	88.89±4
S8	∼	∼	∼	89.70±3	83.84±5	89.72±6	82.83±4
S9	91.44±10	85.91±23	83.75±22	∼	∼	92.26±5	89.90±4
S10	91.46±10	85.90±24	83.86±22	91.70±2	86.87±3	∼	∼
MT	**91.73±9**	**85.94±23**	**84.09±22**	**92.51±2**	**88.89±3**	**92.86±4**	**90.91±3**

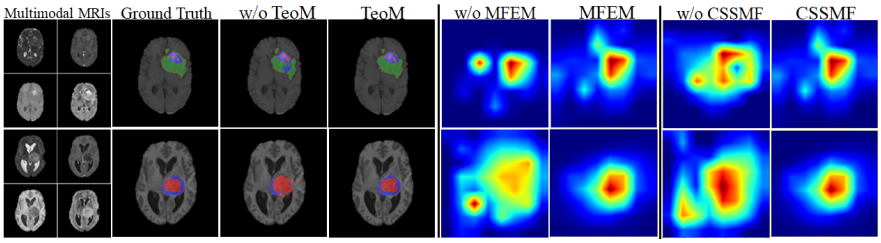

Fig. 4: The Visualization Analysis of MTamba

4 Discussion

We visualize the effectiveness of MTamba, as shown in Fig 4. Specifically, we regard red, green, and purple as the tumor core, edema, and enhancing regions in segmentation, respectively. When inputting multimodal MRIs, using TeoM instead of ToM yields better segmentation output in the edema and enhancing regions. This may be because TeoM can better model the long-range dependencies of MRIs. We use Grad-CAM [15] for feature visualization, and compared to using the features from the segmentation encoder without MFEM, our method focuses more on the tumor and surrounding areas. Features obtained by using summation fusion instead of CSSMF appear more scattered, which may be because CSSMF effectively explores complementary information between features. We also compare DMEM with several feature extractor [10, 5] on the UCSF-PDGM, and DMEM achieves the best performance, surpassing [5] by 4.26% and 5.71% in IDH genotyping and grading AUC, respectively. Compared to other fusion methods [23, 13], CSSMF achieves the best performance. Compared to [23], CSSMF improves WT DICE, IDH genotyping, and grading AUC by 2.28%, 4.84%, and 5.73%, respectively, showing the effectiveness of MTamba.

5 Conclusion

In this paper, we propose a multi-task network named MTamba. This method explores T2-FLAIR mismatch features and is fused with multimodal MRI features extracted from the segmentation encoder for IDH typing and grading. Validated on the publicly available UCSF-PDGM and BraTS2020 datasets, MTamba achieves good performance in segmentation and diagnosis, showing the potential to serve as a reliable computer-aided tool for glioma.

Acknowledgement. This work was supported in part by the Scientific Research Fund of Hunan Provincial Education Department (No. 23A0020), the Science and Technology Major Project of Changsha (No. kh2502004), the Natural Science Foundation of Hunan Province (No. 2025JJ50374), the Central South University Innovation-Driven Research Programme (No. 2023CXQD018) and the High-Performance Computing Center of Central South University.

Disclosure of Interests. The authors declare no conflict of interest.

References

1. Bakas, S., Akbari, H., Sotiras, A., Bilello, M., Rozycki, M., Kirby, J.S., Freymann, J.B., Farahani, K., Davatzikos, C.: Advancing the cancer genome atlas glioma mri collections with expert segmentation labels and radiomic features. Scientific data **4**(1), 1–13 (2017)
2. van den Bent, M.J., French, P.J., Brat, D., Tonn, J.C., Touat, M., Ellingson, B.M., Young, R.J., Pallud, J., von Deimling, A., Sahm, F., et al.: The biological significance of tumor grade, age, enhancement, and extent of resection in idh-mutant gliomas: How should they inform treatment decisions in the era of idh inhibitors? Neuro-oncology **26**(10), 1805–1822 (2024)
3. Calabrese, E., Villanueva-Meyer, J.E., Rudie, J.D., Rauschecker, A.M., Baid, U., Bakas, S., Cha, S., Mongan, J.T., Hess, C.P.: The university of california san francisco preoperative diffuse glioma mri dataset. Radiology: Artificial Intelligence **4**(6), e220058 (2022)
4. Cheng, J., Liu, J., Kuang, H., Wang, J.: A fully automated multimodal mri-based multi-task learning for glioma segmentation and idh genotyping. IEEE Transactions on Medical Imaging **41**(6), 1520–1532 (2022)
5. Cui, H., Ruan, Z., Xu, Z., Luo, X., Dai, J., Geng, D.: Resmt: A hybrid cnn-transformer framework for glioma grading with 3d mri. Computers and Electrical Engineering **120**, 109745 (2024)
6. Dagher, S.A., Lochner, R.H., Ozkara, B.B., Schomer, D.F., Wintermark, M., Fuller, G.N., Ucisik, F.E.: The t2-flair mismatch sign in oncologic neuroradiology: History, current use, emerging data, and future directions. The Neuroradiology Journal **37**(4), 441–453 (2024)
7. Decuyper, M., Bonte, S., Deblaere, K., Van Holen, R.: Automated mri based pipeline for segmentation and prediction of grade, idh mutation and 1p19q co-deletion in glioma. Computerized Medical Imaging and Graphics **88**, 101831 (2021)

8. Doniselli, F.M., Pascuzzo, R., Mazzi, F., Padelli, F., Moscatelli, M., Akinci DAntonoli, T., Cuocolo, R., Aquino, D., Cuccarini, V., Sconfienza, L.M.: Quality assessment of the mri-radiomics studies for mgmt promoter methylation prediction in glioma: a systematic review and meta-analysis. European Radiology pp. 1–14 (2024)
9. Gu, A., Dao, T.: Mamba: Linear-time sequence modeling with selective state spaces. arXiv preprint arXiv:2312.00752 (2023)
10. Hizukuri, A., Tanaka, D., Nakayama, R., Kusuda, K., Masamune, K., Muragaki, Y.: Computerized classification method for molecular subtypes of low-grade gliomas on brain mr images using modified arcface with gram–schmidt orthogonalization. IEEE Access (2024)
11. Jain, R., Johnson, D.R., Patel, S.H., Castillo, M., Smits, M., van den Bent, M.J., Chi, A.S., Cahill, D.P.: real world use of a highly reliable imaging sign:t2-flair mismatch for identification of idh mutant astrocytomas. Neuro-oncology **22**(7), 936–943 (2020)
12. Kendall, A., Gal, Y., Cipolla, R.: Multi-task learning using uncertainty to weigh losses for scene geometry and semantics. In: Proceedings of the IEEE conference on computer vision and pattern recognition. pp. 7482–7491 (2018)
13. Pan, J.: Differential diagnosis of low-and high-grade gliomas using radiomics and deep learning fusion signatures based on multiple magnetic resonance imaging sequences. Journal of Biotech Research **17**, 146–158 (2024)
14. Patel, S.H., Poisson, L.M., Brat, D.J., Zhou, Y., Cooper, L., Snuderl, M., Thomas, C., Franceschi, A.M., Griffith, B., Flanders, A.E., et al.: T2–flair mismatch, an imaging biomarker for idh and 1p/19q status in lower-grade gliomas: a tcga/tcia project. Clinical cancer research **23**(20), 6078–6085 (2017)
15. Selvaraju, R.R., Cogswell, M., Das, A., Vedantam, R., Parikh, D., Batra, D.: Grad-cam: visual explanations from deep networks via gradient-based localization. International journal of computer vision **128**, 336–359 (2020)
16. Sun, X., Li, S., Ma, C., Fang, W., Jing, X., Yang, C., Li, H., Zhang, X., Ge, C., Liu, B., et al.: Glioma subtype prediction based on radiomics of tumor and peritumoral edema under automatic segmentation. Scientific Reports **14**(1), 27471 (2024)
17. Tupe-Waghmare, P., Adithya, S.V., Bhaskar, N.: A multi-task cnn model for automated prediction of isocitrate dehydrogenase mutation status and grade of gliomas. Mathematical Modelling of Engineering Problems **11**(5) (2024)
18. van der Voort, S.R., Incekara, F., Wijnenga, M.M., Kapsas, G., Gahrmann, R., Schouten, J.W., Nandoe Tewarie, R., Lycklama, G.J., De Witt Hamer, P.C., Eijgelaar, R.S., et al.: Combined molecular subtyping, grading, and segmentation of glioma using multi-task deep learning. Neuro-oncology **25**(2), 279–289 (2023)
19. Wang, Y., Wang, Y., Guo, C., Zhang, S., Yang, L.: Sgpnet: A three-dimensional multitask residual framework for segmentation and idh genotype prediction of gliomas. Computational Intelligence and Neuroscience **2021**(1), 5520281 (2021)
20. Weller, M., Wen, P.Y., Chang, S.M., Dirven, L., Lim, M., Monje, M., Reifenberger, G.: Glioma (primer). Nature Reviews: Disease Primers **10**(1), 33 (2024)
21. Wright, L., Demeure, N.: Ranger21: a synergistic deep learning optimizer. arXiv preprint arXiv:2106.13731 (2021)
22. Xing, Z., Ye, T., Yang, Y., Liu, G., Zhu, L.: Segmamba: Long-range sequential modeling mamba for 3d medical image segmentation. In: International Conference on Medical Image Computing and Computer-Assisted Intervention. pp. 578–588. Springer (2024)

23. Yao, J., Liu, J., Cheng, J., Kuang, H., Wang, J.: M 3 ci-net: Multi-modal mri-based characteristics inspired network for idh genotyping. In: 2023 IEEE International Conference on Bioinformatics and Biomedicine (BIBM). pp. 1649–1654. IEEE (2023)
24. Zhang, J., Cao, J., Tang, F., Xie, T., Feng, Q., Huang, M.: Multi-level feature exploration and fusion network for prediction of idh status in gliomas from mri. IEEE Journal of Biomedical and Health Informatics **28**(1), 42–53 (2023)